IN-PLANE BULK ACOUSTIC RESONATORS USING 50NM-THICK NANO-LAMINATED FERROELECTRIC $HF_{0.5}ZR_{0.5}O_2$

Troy Tharpe, Faysal Hakim, and Roozbeh Tabrizian
Department of Electrical and Computer Engineering, University of Florida, Gainesville, FL, USA

2021 21st International Conference on Solid-State Sensors, Actuators and Microsystems (Transducers) | 978-1-6654-1267-4/21/$31.00 ©2021 IEEE | DOI: 10.1109/TRANSDUCERS50396.2021.9495745

ABSTRACT

This paper reports, for the first time, on the use of thickness-scalable nano-laminated ferroelectric hafnium zirconium oxide ($Hf_{0.5}Zr_{0.5}O_2$) films to realize high quality factor (Q), in-plane bulk, acoustic wave (BAW) resonators. 50nm-thick nano-laminated $Hf_{0.5}Zr_{0.5}O_2$ transducers are created from growth interruption of 10nm-thick $Hf_{0.5}Zr_{0.5}O_2$ layers by 1nm-thick aluminum oxide interlayers, enabling thickness scaling of the transducer beyond the ~20nm fundamental limit of ferroelectric orthorhombic crystal phase. The thickness scaling of the $Hf_{0.5}Zr_{0.5}O_2$ transducer results in substantial enhancement of resonator Q and power handling, while sustaining ferroelectric switchability and piezoelectric coupling. Various resonator prototypes, with lithographically scaled frequencies, are implemented in the same batch, showing resonance frequencies over 108 – 691 MHz, mechanical Qs exceeding 500, and $f_{res} \times Q$ products up to 1.84×10^{11}.

KEYWORDS

Nano-laminated, ferroelectric, hafnium zirconium oxide, bulk acoustic wave resonator.

INTRODUCTION

Monolithic integration of high-quality factor (Q) nano-mechanical resonators with CMOS solid-state electronics provide transformative impact on various performance and integration merits for frequency control microsystems, such as radio-frequency oscillators and spectral processors. These include significant reduction in insertion loss, impedance, interference/crosstalk, system form-factor and power consumption. More specifically, with the increasing adoption of spread-spectrum communication and clock-generation schemes in wireless communication systems and microprocessors, non-monolithic frequency generation and control solutions impose substantial scalability limitations, especially at higher frequencies.

The major challenge with monolithic integration of nano-mechanical resonators has been the lack of an integrated transducer that: (a) is truly compatible for integration within or post-CMOS, and (b) provides large coupling and high Q needed to create high performance RF filters and stable oscillators.

The discovery of ferroelectric behavior in atomically engineered hafnia [1], along with the recent demonstration of hafnia-based nano-electro-mechanical transducers [2-5], augurs a potential solution for realization of monolithically integrated high-Q nano-mechanical resonators.

Hafnia has been adopted over the past two-decades as a CMOS compatible, standard high-k dielectric which can be easily tailored (with low-thermal budgets) to provide ferroelectric behavior and large piezoelectric properties. The ferroelectric behavior in atomically engineered hafnia corresponds to the formation of meta-stable orthorhombic crystal phase through thermomechanical engineering of the film at atomic scale. While very large piezoelectric constants are measured for ferroelectric hafnia [3], the major challenge in realization of high-performance nano-mechanical resonators is the fundamental thickness-scaling limit [6-7]. The meta-stable orthorhombic phase, that is responsible for ferroelectricity, is only sustained for film thicknesses lower than 15-20nm. Exceeding this thickness limit promotes the growth of non-ferroelectric crystal phases which reduce the piezoelectric coupling of the transducer. This is particularly undesirable for mechanical resonator applications, where sub-20nm films are too thin to provide / sustain the effective transduction efficiency, Q, and power-handling desired.

This paper reports, for the first time, on the use of nano-lamination for thickness scaling of ferroelectric hafnium zirconium oxide ($Hf_{0.5}Zr_{0.5}O_2$) transducers beyond the fundamental thickness limit, and creation of high-Q lateral bulk acoustic wave resonators. Nano-laminated transducers are created by interrupting ~10nm $Hf_{0.5}Zr_{0.5}O_2$ layers with 1nm aluminum oxide (Al_2O_3) interlayers to prevent formation of non-ferroelectric crystal phases upon thickness scaling. 0.1 – 0.7 GHz BAW resonators are created in 50nm nano-laminated $Hf_{0.5}Zr_{0.5}O_2$, showing Qs exceeding 500, and $f_{res} \times Q$ products as high as $\sim 2 \times 10^{11}$.

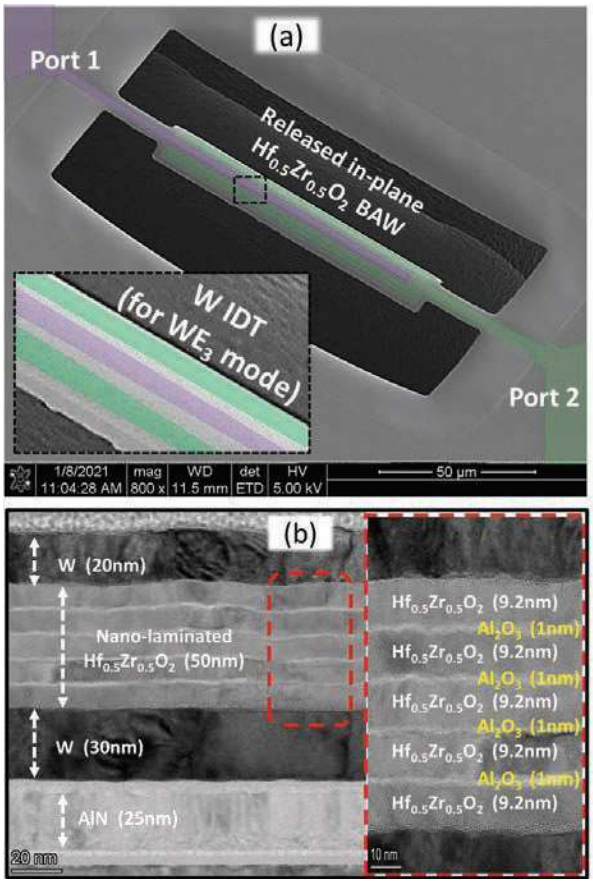

Fig. 1. (a) Scanning electron microscope (SEM) image of nano-laminated $Hf_{0.5}Zr_{0.5}O_2$ BAW resonator; (b) its cross-sectional transmission electron microscope (TEM) image.

NANO-LAMINATED $Hf_{0.5}Zr_{0.5}O_2$

Interposing Al_2O_3 layers between orthorhombic $Hf_{0.5}Zr_{0.5}O_2$ thin films enables creation of laminate transducers with stable remnant polarization (P_R) values independent of the thickness, significantly reducing leakage current, and improving thermal stability [8]. In this work, nano-lamination is achieved using a Cambridge NanoTech Fiji 200 atomic layer deposition (ALD) system with a process set point of 200°C. $Hf_{0.5}Zr_{0.5}O_2$ layers are deposited using Tetrakis(dimethylamido)hafnium(IV) (TDMAH) and Tetrakis(dimethylamido)zirconium(IV) (TDMAZ) precursors with a cycle ratio of 1:1. Application of O_2 then H_2 plasmas allows for monolayer oxidation and promotes the formation of orthorhombic crystalline phases during subsequent Rapid Thermal Anneal (RTA) [9]. This process then repeats to form a single $Hf_{0.5}Zr_{0.5}O_2$ layer of ~10nm. Al_2O_3 interlayers are formed via thermal ALD using ten cycles of TriMethylAluminum (TMA) precursor resulting in ~1nm of growth. Deposition steps are next cycled three additional times, followed by a top deposition of ~10nm $Hf_{0.5}Zr_{0.5}O_2$ to form the complete ~50nm laminate transducer.

Formation of $Hf_{0.5}Zr_{0.5}O_2$ is inherently amorphous due to insufficient thermal budget within the process chamber. Therefore, creation of a non-centrosymmetric orthorhombic crystalline phase, responsible for film ferroelectricity, requires RTA within a stress constrained environment [4]. To provide this constrained environment, 20nm of titanium nitride (TiN) is deposited using Tetrakis(dimethylamido)titanium(IV) precursor while exposed to nitrogen plasma. The complete structure, including capping TiN and bottom Tungsten (W) electrode, is then subject to 20s RTA at 500°C in N_2 ambient. Following RTA, TiN is stripped in 3min of heated H_2O_2 solution, and replaced with 20nm of DC sputtered W. Fig. 1 (b) depicts cross-sectional Transmission Electron Microscope (TEM) images of the finalized nano-laminate film. Fig. 1 (b) also shows the laminate film in relation to other device layers, while the zoomed inset highlights the $Hf_{0.5}Zr_{0.5}O_2$-Al_2O_3 super lattice.

FABRICATION PROCESS

Fig. 2 summarizes the fabrication process flow utilized to produce lithographically scalable, nano-laminated $Hf_{0.5}Zr_{0.5}O_2$ BAW resonators.

25nm of aluminum nitride (AlN) is first sputtered atop a silicon (Si) substrate to serve as a resonant structural layer and etch inhibitor during release. Next, a 30nm W layer is sputtered and patterned using a liftoff process to form device ground (GND) electrodes. 200nm-thick W pads are also formed using this same process to reduce contact resistance during probing. Next, the $Hf_{0.5}Zr_{0.5}O_2$ - Al_2O_3 nano-laminated transducer and the capping TiN layer are deposited via ALD according to process conditions described in the section prior. RTA is then performed, followed by removing the TiN layer via heated hydrogen peroxide. Nano-laminate $Hf_{0.5}Zr_{0.5}O_2$ is then Reactive Ion Etched (RIE) using a Cl_2 /Ar gas chemistry to open access to thick bottom W pads. Subsequently, top electrodes are formed by sputtering 20nm W and lifting off to form device top electrodes. 200nm-thick platinum (Pt) pads are next

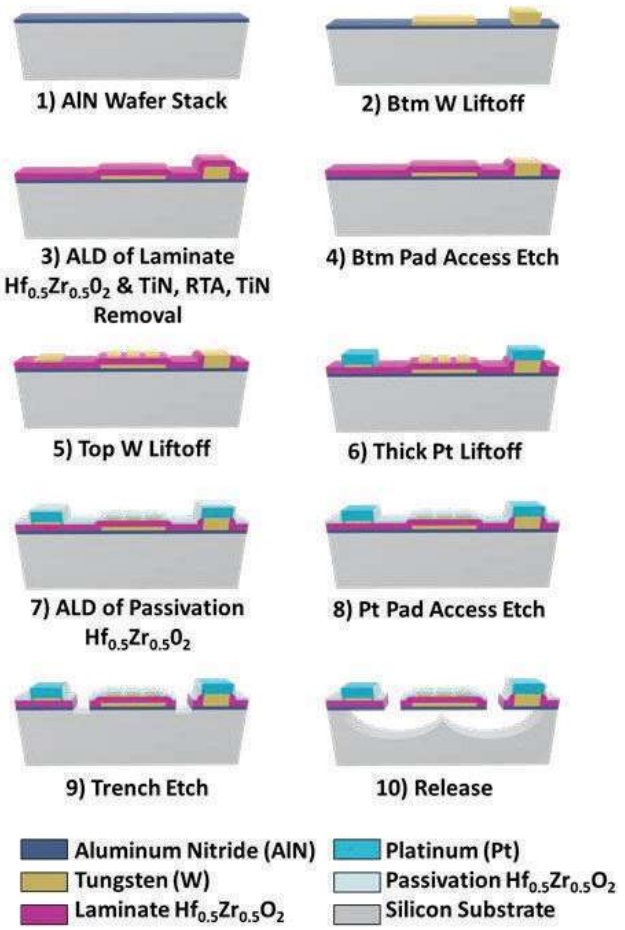

Fig. 2: Fabrication process flow for nano-laminated $Hf_{0.5}Zr_{0.5}O_2$ on AlN BAW resonators.

deposited and pattered in similar fashion to provide a solid, low resistance contact point. To protect top electrode W from etching during sulfur hexafluoride (SF_6) release, a conformal ALD of 20nm $Hf_{0.5}Zr_{0.5}O_2$ is performed to serve as a passivation layer. This passivation layer is then removed by RIE to expose underlying Pt. Trenches defining resonator lateral geometry are then etched again using RIE, with care being taken to ensure slight over etch into Si substrate. After trench etching, the device is released using a high density SF_6 plasma, with bottom Si substrate serving as a sacrificial layer, and the starting AlN layer serving as an etch stop.

BAW RESONATOR DESIGN

Rectangular resonators, connected to the substrate with narrow tethers, are designed for the excitation of odd order Width Extensional (WE) modes, with electrode topology varied to target the excitation of 1st (Fig. 3 (a)), and 3rd (Fig. 3 (b)) WE modes.

Odd order WE resonance frequencies of the above laminate ferroelectric BAW resonator can be defined by:

$$f_n = \frac{n}{2W_0}\sqrt{\frac{E_{Eq}}{\rho_{Eq}}} \quad (1).$$

Here n is the odd mode number of excitation, W_0 is the device width, E_{Eq} is the equivalent young's modulus of the

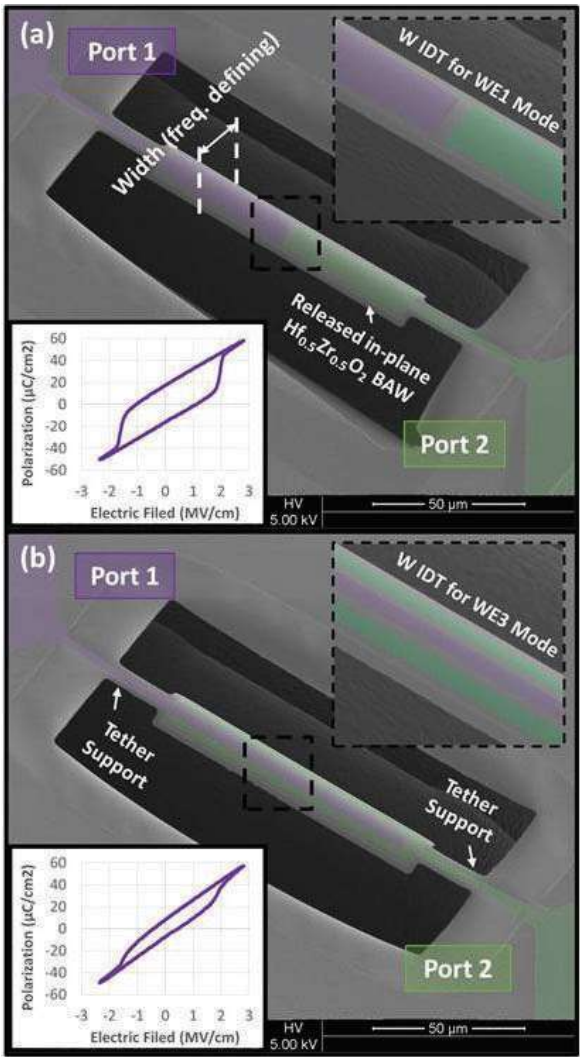

Fig. 3: (a) Released, in-plane, laminated, $Hf_{0.5}Zr_{0.5}O_2$ *BAW resonator with* WE_1 *electrode configuration (inset right) and polarization vs electric field hysteresis loop taken at Port 1 (inset left). (b) Released, in-plane, laminated,* $Hf_{0.5}Zr_{0.5}O_2$ *BAW resonator with* WE_3 *electrode configuration (inset right) and polarization vs electric field hysteresis loop taken at Port 1 (inset left).*

resonant stack, and ρ_{Eq} is the resonator's equivalent density. From Eq. (1) it is evident that device width can effectively be utilized to scale resonator operating frequency in a lithographically defined manner.

All fabricated devices consist of a 30nm AlN structural layer, 30nm bottom tungsten electrodes, a 50nm nano-laminated $Hf_{0.5}Zr_{0.5}O_2$ transducer, 20nm top tungsten electrodes, and a 20nm top $Hf_{0.5}Zr_{0.5}O_2$ passivation layer for protection during release. The top right insets of Fig. 3 (a) and Fig. 3 (b) highlight the top W electrodes used for drive and sense. While the bottom left insets of Fig. 3 (a) and Fig. 3 (b) depict the polarization hysteresis loop of each device's nano-laminate transducer, measured at Port 1 after the application of 1,000 cycles of a 13V, 1kHz square wakeup pulse. Devices are varied to include 10um, 20um (depicted in Fig. 3 (a) and Fig. 3 (b)), and 30um widths. Device lengths are held constant at 100um to further exemplify the effect of width and electrode topology on resonant frequency.

RESONATOR CHARACTERIZATION

Prior to RF transmission line measurement, a Radiant PiezoMEMS analyzer is used to apply a 13V, 1kHz square wakeup pulse. This wakeup pulse is designed to convert remaining tetragonal phases to orthorhombic, and de-pin domains [10] yielding the hysteretic polarization loops displayed within Fig. 3 (a) and Fig. 3 (b) insets and promoting transduction. This measurement and corresponding bipolar waveform applied to both device ports inherently places each in a down polarized state. A Keysight N5222A vector network analyzer is then used to measure the forward transmission coefficient (S_{21}) for devices with 10um, 20um, and 30um widths, and electrode configurations targeting WE_1 And WE_3 modes.

To eliminate the effect of electrical feedthrough on mechanical Q, it is necessary to measure and subtract transmission responses under opposing ferroelectric polarization scenarios. This is achieved by first measuring transmission coefficients with both device ports polarized in a negative state ($S_{21}^{-P_R}$). Polarization state on one device port is then flipped to the positive state and the measurement is repeated, yielding $S_{21}^{+P_R}$. Given:

$$S_{21}^{+P_R} \propto (i_m + i_{FT}) \quad (2),$$

and,

$$S_{21}^{-P_R} \propto (-i_m + i_{FT}) \quad (3),$$

it follows that:

$$S_{21}^{FT\ Correct} \propto i_m \propto \frac{S_{21}^{+P_R} - S_{21}^{-P_R}}{2} \quad (4).$$

Here, i_m is the current through the motional branch (device), i_{FT} is the feed through current, and $S_{21}^{FT\ Correct}$ is the feedthrough corrected forward transmission response.

Fig. 4 (a-d) depicts $S_{21}^{FT\ Correct}$ for varied width, single finger (WE_1) electrode topology devices. Fig. 4 (a) shows the large span frequency response for WE_1 electroded

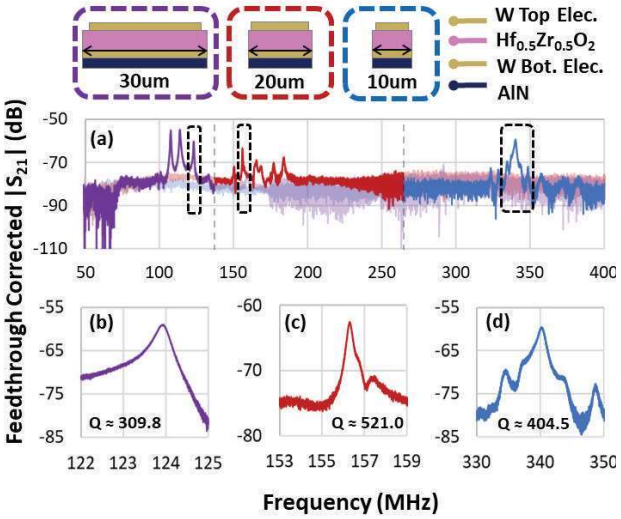

Fig. 4: (above) Color keyed legend mapping response to device width. (a) Large span frequency response for 30um, 20um, and 10um devices with single finger WE_1 *electrode topology. (b-d) Short span frequency response of regions highlighted above.*

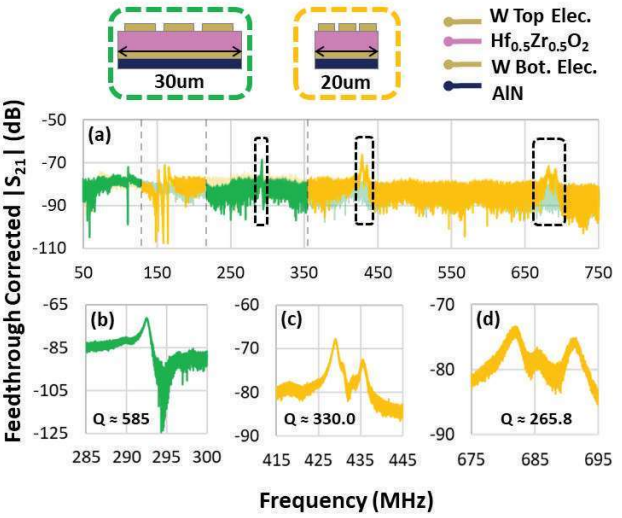

Fig. 5: (above) Color keyed legend mapping response to device width. (a) Large span frequency response for 30um and 20um devices with three finger WE_3 electrode topology. (b-d) Short span frequency response of regions highlighted above.

devices. Fig. 4 (b-d) present short span frequency responses for single finger devices operating at WE_1. The color-coded legend above Fig. 4 (a) correlates all width combinations with their associated responses.

Fig. 5 (a-d) depicts $S_{21}^{FT\ Correct}$ for 30um and 20um width devices with WE_3 electrode configurations. Fig. 5 (a) shows the large span frequency response for these devices. Fig. 5 (b-d) present short span frequency responses for three finger devices operating at WE_3 and WE_5. The color-coded legend above Fig. 5 (a) correlates all width combinations with their associated responses.

CONCLUSION

This work reports, for the first time, on the use of nano-laminated $Hf_{0.5}Zr_{0.5}O_2$ transducers for the realization of in-plane BAW resonators. By utilizing nano-lamination, this paper presents a method to overcome thickness scalability limitations of previously reported $Hf_{0.5}Zr_{0.5}O_2$ transducers, enabling enhancement of resonator Q and power handling. Lateral BAW resonators with 50nm-thick nano-laminated $Hf_{0.5}Zr_{0.5}O_2$ transducers are presented with frequencies over $0.1-0.7$ GHz, Qs higher than 500, and $f_{res}\times Q$ products as high as $\sim 2\times 10^{11}$. The promise of monolithic integration, large piezoelectric coefficients, and intrinsic switchability of $Hf_{0.5}Zr_{0.5}O_2$, combined with the enhancement of resonator Q by nano-lamination thickness scalability, position ferroelectric $Hf_{0.5}Zr_{0.5}O_2$ BAW resonators as an attractive technology for spectral processing and reference generation in spread-spectrum electronic systems.

ACKNOWLEDGEMENTS

This project is supported by DARPA Young Faculty Award program. The authors would like to thank DARPA program manager Dr. Timothy Hancock for his support of this work.

REFERENCES

[1] T. S. Böscke, J. Müller, D. Bräuhaus, U. Schröder, and U. Böttger, "Ferroelectricity in hafnium oxide thin films," *Appl. Phys. Lett.*, vol. 99, no. 10, 2011, doi: 10.1063/1.3634052.

[2] M. Ghatge, G. Walters, T. Nishida, and R. Tabrizian, "An ultrathin integrated nanoelectromechanical transducer based on hafnium zirconium oxide," *Nat. Electron.*, vol. 2, no. 11, pp. 506–512, 2019, doi: 10.1038/s41928-019-0305-3.

[3] M. Ghatge, G. Walters, T. Nishida, and R. Tabrizian, "A Nano-Mechanical Resonator with 10nm Hafnium-Zirconium Oxide Ferroelectric Transducer," *Tech. Dig. - Int. Electron Devices Meet. IEDM*, vol. 2018-Decem, pp. 4.6.1-4.6.4, 2019, doi: 10.1109/IEDM.2018.8614633.

[4] M. Ghatge, G. Walters, T. Nishida, and R. Tabrizian, "A 30-nm thick integrated hafnium zirconium oxide nano-electro-mechanical membrane resonator," *Appl. Phys. Lett.*, vol. 116, no. 4, 2020, doi: 10.1063/1.5134856.

[5] F. Hakim, M. Ghatge, and R. Tabrizian, "Excitation of high-frequency in-plane bulk acoustic resonance modes in geometrically engineered hafnium zirconium oxide nano-electro-mechanical membrane," *Appl. Phys. Lett.*, vol. 117, no. 6, pp. 1–6, 2020, doi: 10.1063/5.0016347.

[6] M. H. Park *et al.*, "Study on the degradation mechanism of the ferroelectric properties of thin Hf0.5Zr0.5O2 films on TiN and Ir electrodes," *Appl. Phys. Lett.*, vol. 105, no. 7, pp. 0–5, 2014, doi: 10.1063/1.4893376.

[7] H. J. Kim *et al.*, "Grain size engineering for ferroelectric Hf0.5Zr0.5O2 films by an insertion of Al2O3 interlayer," *Appl. Phys. Lett.*, vol. 105, no. 19, pp. 1–6, 2014, doi: 10.1063/1.4902072.

[8] S. Riedel, P. Polakowski, and J. Müller, "A thermally robust and thickness independent ferroelectric phase in laminated hafnium zirconium oxide," vol. 095123, no. June, 2016, doi: 10.1063/1.4964300.

[9] G. Walters, A. Shekhawat, S. Moghaddam, J. L. Jones, and T. Nishida, "Effect of in situ hydrogen plasma on the ferroelectricity of hafnium zirconium oxide films," *Appl. Phys. Lett.*, vol. 116, no. 3, 2020, doi: 10.1063/1.5135709.

[10] S. S. Fields *et al.*, "Phase-Exchange-Driven Wake-Up and Fatigue in Ferroelectric Hafnium Zirconium Oxide Films," *ACS Appl. Mater. Interfaces*, vol. 12, no. 23, pp. 26577–26585, 2020, doi: 10.1021/acsami.0c03570.

CONTACT

Troy Tharpe, tel: +1-321-4329557; ttharpe@ufl.edu.